OPTO-ELECTRONICS REVIEW **12**(4), 369–376

Spatial separation of recombining carriers within nitride GaN/(AlGa)N quantum wells induced by piezoelectric phenomena

J. GALCZAK[1], R.P. SARZAŁA[1] and W. NAKWASKI[*1,2]

[1]Laboratory of Computer Physics, Institute of Physics, Technical University of Łódź
219 Wólczańska Str., 93-005 Łódź, Poland
[2]Center for High Technology Materials, University of New Mexico
Albuquerque, NM 87106, 1313 Goddard SE, USA

Nitride $A^{III}N$ materials manifest very strong piezoelectric effects. Their piezoelectric coefficients are one order of magnitude higher than those in similar $A^{III}B^{V}$ semiconductors. Therefore stress fields, generated for example at nitride heterojunctions, because of different lattice constants of their both components, are followed by an additional piezoelectric polarization and some local curving of band edges. In quantum wells (QWs), on the other hand, this stress-related piezoelectric polarization and, additionally, the spontaneous polarization are sources of an electric field which causes the so-called quantum confined Stark effect, leading to an effective band-gap shrinkage and spatial separation of electrons and holes. Both the above phenomena influence considerably recombination processes in QW devices. The last effect, i.e. the stress-induced spatial separation of electrons and holes confined within nitride QWs, is investigated theoretically in the present paper. Electron transitions from its ground state to the second heavy-hole state have been found to play much more considerable role in recombination phenomena within wider nitride QWs than it has been expected.

Keywords: polarization phenomena, **k·p** method, nitride quantum-well devices, envelope functions.

1. Introduction

During last few years, $A^{III}N$ nitride semiconductors and their ternary compounds have attracted considerable attention, and turned out to be ones of the most promising materials in modern electronics and optoelectronics. Their energy gaps (ranging from 1.9 eV to as much as 6.2 eV) make them ideal candidates for devices detecting and emitting radiation from visible red to ultraviolet. Though many successful attempts were made to understand and describe physical and operating properties of devices based on those materials, there are still some unsolved problems. One of them is a very strong piezoelectric effect [1–4].

Differences of lattice constants at heterojunctions of nitride quantum-well (QW) devices are sources of stresses in a crystal lattice, which is followed by some piezoelectric polarization. This stress-induces polarization together with spontaneous polarization cause electric fields [5] in the QW region, which is called quantum confined stark effect [6–8].

To analyse the influence of piezoelectric polarization on behaviour of recombining carriers, the modified (to include polarization phenomena) version of the **k·p** method, based on the approach of Chuang and Chang [9–11] to wurtzite semiconductors, is used to examine shapes of electron and hole envelope functions in the neighbourhood of the GaN quantum well confined by the $Al_xGa_{1-x}N$ barriers. Integral overlap of these envelope functions is then calculated to allow future observations of influence of the stress-induced polarization on optical properties of $A^{III}N$ nitride devices, which depends on square of the integral overlap.

2. The theory

To include possible polarization effects in the strained wurtzite semiconductor crystals, the additional Hamiltonian term $P_E(z)$ has to be taken into account

$$P_E(z) = q_e E(z) z, \tag{1}$$

where q_e is the electron charge and $E(z)$ is the electric-field distribution in the z-direction perpendicular to the xy p-n junction plane

$$E(z) = \begin{cases} E_W & \text{within the QW} \\ E_B & \text{within the barrier} \end{cases}. \tag{2}$$

The electron envelope functions $\phi_n(z)$ in the conduction band at $k_t = 0$ can be then determined by solving the following eigenvector problem

*e-mail: nakwaski@p.lodz.pl

$$\left[H^C\left(k_t = 0, k_z = -i\frac{\partial}{\partial z}\right) + E_C^0(z) + P_E(z)\right]\phi_n(z) = E_n^c\phi_n(z), \quad (3)$$

where

$$\hat{H}^C\left(k_t, k_z = -i\frac{\partial}{\partial z}\right) = \frac{\hbar^2}{2m_e^t}k_t^2 + \frac{\hbar^2}{2m_e^z}k_z^2 + P_{c\varepsilon} \quad (4)$$

and where additionally an impact of mechanical stresses and induced electrical fields is included. In the above equations, E_n^c is the energy of the nth conduction-band electron, the wave-vector component k_t on the xy plane parallel to the p-n junction is related to its k_x and k_y components: $k_t^2 = k_x^2 + k_y^2$, k_z wave-vector component is perpendicular to the p-n junction plane, $E_C^0(z)$ is the potential energy profile of the conduction-band edge in the un-strained QW and $P_{c\varepsilon}$ stands for the hydrostatic energy shift in the conduction band induced by mechanical stresses, which in this particular case (wurtzite material) is for simplicity (ignoring wurtzite crystal anisotropy) expressed as

$$P_{c\varepsilon} = 2a_c\varepsilon_{11}\left(1 - \frac{C_{13}}{C_{33}}\right), \quad (5)$$

where a_c is the conduction band deformation potential, ε_{11} stands for the strain within the p-n junction plane and C_{13} and C_{33} are the elastic constants (see Table 1).

Table. 1. Some physical parameters of the GaN and the AlN binary compounds [1,12,13].

Parameter	Unit	GaN	AlN
Lattice constants			
a	Å	3.199	3.11
c	Å	5.226	4.99
Dielectric constants			
ε	F/m	8.9	8.5
Piezoelectric constants			
e_{31}	C/m^2	–0.49	–0.60
e_3	C/m^2	0.73	1.46
Elastic stiffness constants			
C_{13}	GPa	103	108
C_{33}	GPa	405	373

Analogous eigenvector problem equations for a hole within the degenerate valence sub-bands at $k_t = 0$ may be then expressed as

$$\left[H_{ij}^U\left(k_z = -i\frac{\partial}{\partial z}\right) + \delta_{ij}\left(E_V^0(z) + P_E(z)\right)\right]g_m^{(i)}(z) = E_m^U(z)g_m^{(i)}(z), \quad (6)$$

$$\left[H_{ij}^L\left(k_z = -i\frac{\partial}{\partial z}\right) + \delta_{ij}\left(E_V^0(z) + P_E(z)\right)\right]g_m^{(i)}(z) = E_m^L(z)g_m^{(i)}(z), \quad (7)$$

where the upper H^U and the lower H^L valence-band Hamiltonians are components of the $H_{6\times6}$ block-diagonalized Hamiltonian proposed by Chuang and Chang [9] (see Appendix A), δ_{ij} stands for the Kronecker delta, $E_V^0(z)$ is the valence-band reference energy, and $g_m^{(i)}$ (i = 1,4 – heavy holes (hh); 2,5 – light holes (lh); 3,6 – crystal split-off holes (ch)) are the envelope functions of the mth valence band hole.

3. The polarization induced electric fields

Let us consider the $Al_xGa_{1-x}N/GaN/Al_xGa_{1-x}N$ quantum well (Fig. 1) for which material parameters are available (Table 1) and some experimental results have been reported. The GaN QW of the width L_W is assumed to be much thinner than both the $Al_xGa_{1-x}N$ barriers of the width L_B, therefore misfit-induced stresses may be assumed to be confined to the quantum well only. The 0z co-ordinate is perpendicular to the well/barrier interfaces and directed along the crystallographic [0001] axis. Therefore spontaneous polarization vectors $\mathbf{P}^{SP}$ are directed in the opposite direction of the 0z axis (Fig. 1). Their values can be obtained from the following relation [12]

$$P_{AlGaN}^{SP} = -0.090 - 0.034(1-x) + 0.021x(1-x) \ \ (\mathrm{C/m^2}). \quad (8)$$

Mismatch-related stress-induced piezoelectric field P^{PZ} within the $Al_xGa_{1-x}N/GaN/Al_xGa_{1-x}N$ quantum well have only one nonzero component, which is directed along 0z axis and can be expressed as

$$P^{PZ} = 2\frac{a_{AlGaN} - a_{GaN}}{a_{GaN}}\left(e_{31} - e_{33}\frac{C_{13}}{C_{33}}\right), \quad (9)$$

where e_{ij} are piezoelectric constants and a_{AlGaN} and a_{GaN} are lattice constants of the Al_xGa_{1-x} and the GaN materials, respectively. Following Ref. 5, the total electric fields within the quantum well E_W and within the barriers E_B may be written as

$$E_W = \frac{P_{AlGaN}^{SP} - P_{GaN}^{SP} - P_{GaN}^{PZ}}{\varepsilon_0\left(\varepsilon_W + \varepsilon_B\frac{L_W}{2L_B}\right)}, \quad (10)$$

$$E_B = \frac{P_{GaN}^{SP} + P_{GaN}^{PZ} - P_{AlGaN}^{SP}}{\varepsilon_0\left(\varepsilon_B + 2\varepsilon_W\frac{L_B}{L_W}\right)}, \quad (11)$$

where ε_0 is the free-space dielectric constant and ε_W and ε_B are the relative dielectric constants of the quantum well and the barrier materials (Table 1). The **k·p** parameters for the binary GaN and AlN compounds are listed in Table 2.

 © 2004 COSiW SEP, Warsaw

Table. 2. The **k·p** parameters of the binary GaN and AlN compounds [11,14,15,16].

Parameter	Unit	GaN	AlN
Energy parameters			
E_g	meV	3440	6280
$\Delta_1 = \Delta_{cr}$	meV	72	–58
$\Delta_{so} = 3\Delta_2 = 3\Delta_3$	meV	15	20
Conduction band effective masses			
m_e^z/m_0	–	0.20	0.33
m_e^t/m_0	–	0.18	0.25
Valence band effective mass parameters			
A_1	–	–6.56	–3.95
A_2	–	–0.91	–0.27
A_5	–	–3.13	–1.95
Deformation potentials			
a_c	meV	–4080	–4500
D_1	meV	–890	–2890
D_2	meV	4270	4890

4. The band model

Figure 2 presents the band diagram of the GaN/AlN heterojunction. It is known from experiments [17], that the valence-band edge discontinuity is equal to

$$\Delta E_V = 0.8 \pm 0.3 \ \ \text{(eV)}. \tag{12}$$

Because of a different sign of the Δ_1 crystal-field splitting energy in both binary compounds, there are different arrangements of the energy levels: while E_1 is the highest energy level in GaN, E_2 plays analogous role in AlN. So, formally $\Delta E_v = E_1(\text{GaN}) - E_2(\text{AlN})$. But because exactness of the determined ΔE_v value (0.3 eV) is much higher than both the $\Delta_1 = \Delta_{cr}$ and the $\Delta_2 = \Delta_3 = \Delta_{so}/3$ parameters (c.f. Table 2, here Δ_{cr} is crystal-field split and Δ_{so} is the spin-orbit split-off energy), it is enough to assume

$$\Delta E_V = E_V^0(\text{GaN}) - E_V^0(\text{AlN}). \tag{13}$$

Therefore for the assumed $E_V^0(\text{AlN}) = 0, E_V^0(\text{GaN}) = 0.8 \pm 0.3$ eV. For the ternary $Al_xGa_{1-x}N$ compound [11]

$$E_V^0(\text{Al}_x\text{Ga}_{1-x}\text{N}) = xE_V^0(\text{AlN}) + (1-x)E_V^0(\text{GaN}) + b_V x(1-x), \tag{14a}$$

$$E_C^0(\text{Al}_x\text{Ga}_{1-x}\text{N}) = xE_C^0(\text{AlN}) + (1-x)E_C^0(\text{GaN}) + b_C x(1-x), \tag{14b}$$

$$E_g(\text{Al}_x\text{Ga}_{1-x}\text{N}) = xE_g(\text{AlN}) + (1-x)E_g(\text{GaN}) + bx(1-x), \tag{14c}$$

where $b = b_c - b_v = -0.98$ eV as well as b_c and b_v are the so-called bowing parameters. It is known from experiments that ΔE_c is equal to about 33% of the energy difference between fundamental transitions in AlN and GaN, therefore it is reasonable to assume $b_c = -0.67b$ and $b_v = 0.33b$.

It may be finally concluded that band edges in the nitride quantum-well structure under consideration may be written as

$$E_V^0(z) + P_E(z) = \begin{cases} E_V^0(\text{GaN}) + q_e E_W z & \text{within QW} \\ E_V^0(\text{Al}_x\text{Ga}_{1-x}\text{N}) + q_e E_B z & \text{within barriers} \end{cases}. \tag{15a}$$

$$E_C^0(z) + P_E(z) = \begin{cases} E_C^0(\text{GaN}) + q_e E_W z & \text{within QW} \\ E_C^0(\text{Al}_x\text{Ga}_{1-x}\text{N}) + q_e E_B z & \text{within barriers} \end{cases}. \tag{15b}$$

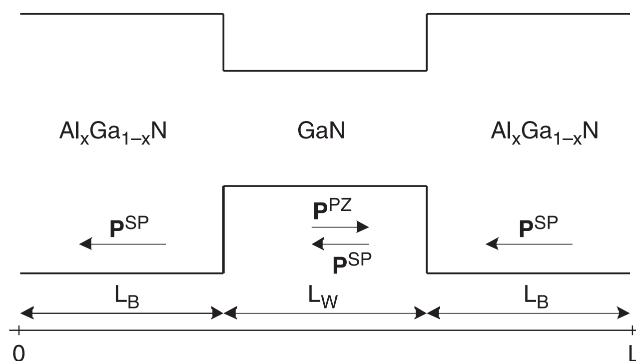

Fig. 1. The band structure of the $Al_xGa_{1-x}N/GaN/Al_xGa_{1-x}N$ quantum well. Vectors of the spontaneous $\mathbf{P}^{SP}$ and the piezoelectric $\mathbf{P}^{PZ}$ polarizations are shown.

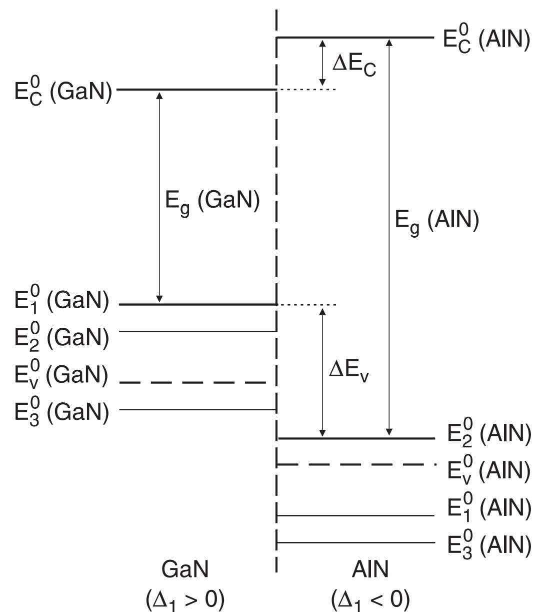

Fig. 2. The band diagram of the GaN/AlN heterojunction. ΔE_C and ΔE_V – the conduction-band and the valence-band, respectively, discontinuities at the heterojunction.

With the exception of the spontaneous (8) and the piezoelectric (9) polarizations, the energy gap (14c), and the band-edge profiles [(15a), (15b)], all values of other material parameters of the $Al_xGa_{1-x}N$ compounds are determined with the aid of a linear interpolation between their values for binary GaN and AlN compounds listed in Table 1 and Table 2.

5. The results

The calculations have been carried out for GaN quantum wells of widths of 2, 3, 4 and 5 nm and 10 nm $Al_xGa_{1-x}N$ barriers with the AlN mole fraction x changing from 0.1 to 1. Currently good-quality $Al_xGa_{1-x}N$ layers of very high AlN contents, grown on GaN layer, are not technologically available, mostly because of crystal cracking [18–20]. Nevertheless, it seems to be worthwhile to consider theoretically their possible influence on prospective device properties.

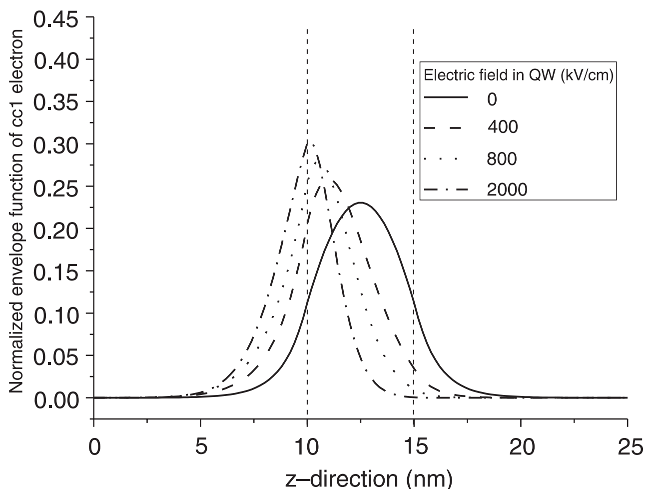

Fig. 3. Normalized envelope functions of the cc1 electrons for various electric fields within the QW.

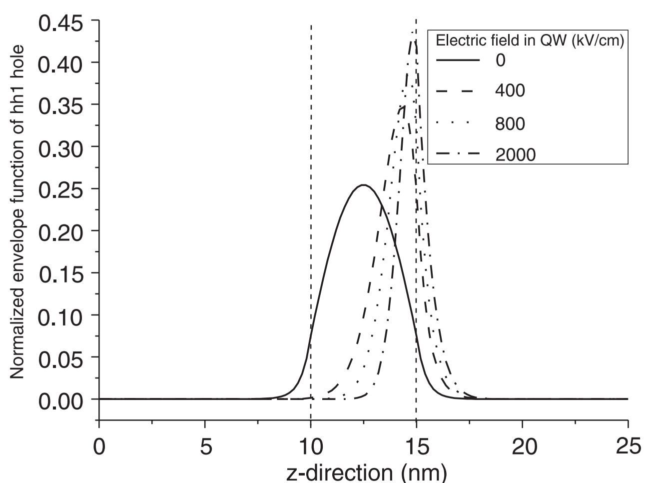

Fig. 4. Normalized envelope functions of the hh1 holes for various electric fields within the QW.

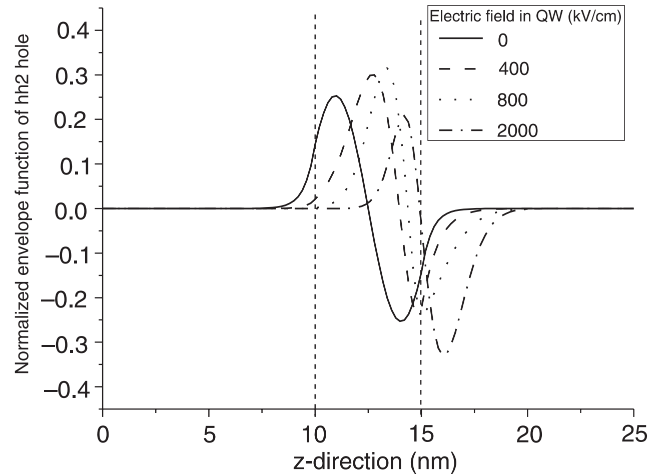

Fig. 5. Normalized envelope functions of the hh2 holes for various electric fields within the QW.

Figures 3, 4, 5, and 6 present shapes of normalized envelope functions ϕ_1 of an electron in the conduction band (cc1), and heavy holes $g_{1,2,3}^{(1,4)}$ in the valence band (hh1, hh2 and hh3) for various electric fields within QW. As it can easily be seen, in the case of neglected polarization effects (solid lines), modules of envelope functions of both groups of carriers are symmetrical with respect to the QW axis. Increasing electric field within QW causes a shift of maxima of the electrons and the holes envelope functions in the opposite directions (dependent on the electric field vector direction) of the QW. The above phenomena, also leading to an effective bang-gap shrinkage and known as a quantum confined Stark effect (QCSE), is directly connected with a steadily increasing difference between lattice constants of the well and the barriers with increasing barriers AlN mole fraction, which means – with stronger piezoelectric polarization causing stronger electric fields in QW (Fig. 7).

To illustrate an influence of piezoelectric polarization on recombination processes in nitride GaN/(AlGa)N QW devices, the theoretical calculations (including polariza-

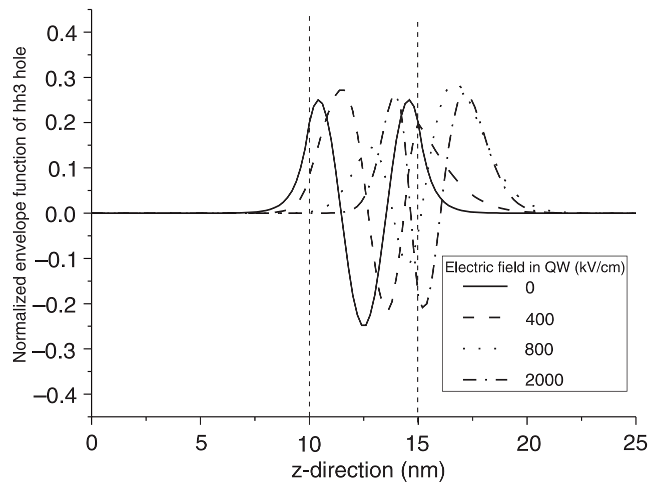

Fig. 6. Normalized envelope functions of the hh3 holes for various electric fields within the QW.

 © 2004 COSiW SEP, Warsaw

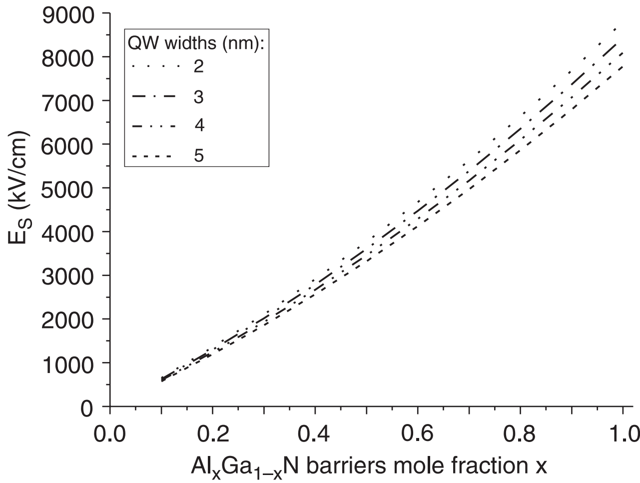

Fig. 7. The electric field E_S within GaN quantum wells of different widths L_S versus the AlN mole fraction x of the 100-Å $Al_xGa_{1-x}N$ barriers.

tion) have been carried out. The electric field of 0.88 MV/cm have been found within the 5-nm-thick well in the structure with 10-nm-thick barriers. Such an electric field causes a very strong carrier separation (QCSE: dashed lines in Fig. 8). As one can see, overlapping of the electron and the hole envelope functions becomes very small resulting in a very low intensity of electron-hole recombination transitions. Of course, carrier separation disappears when the polarization effects are neglected (solid lines in Fig. 8).

To fully understand and not to underestimate the influence of piezoelectric polarization on an operation of nitride QW devices, it is useful to examine the behaviour of square of integral overlap $\left|M_{n,m}^{e-h}\right|^2$ of the electron and the hole envelope functions for different values of an electric field. It is important to stress, that recombination rate is proportional to a square of the integral overlap, which can be defined as follows

$$\left|M_{n,m}^{e-h}\right|^2 = \left|\int_0^L \phi_n(z) g_m^{(i)}(z) dz\right|^2 . \tag{16}$$

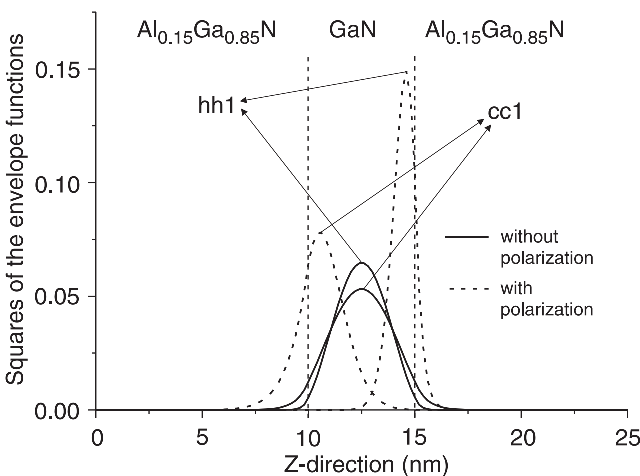

Fig. 8. Squares of the envelope functions for the conduction-band electrons (cc1) and the valence-band heavy holes (hh1) within the 5-nm GaN quantum wells with the 10-nm $Al_{0.2}Ga_{0.8}N$ barriers including polarization (dashed lines) and assuming neglected polarization (solid lines).

Figures 9, 10, 11, and 12 present dependence of the square of the integral overlap of the electron (cc1) and the holes (hh1 and hh2) envelope functions versus electric field in the well for different well widths (2, 3, 4, 5 nm). As expected, at zero electric field, squares of integral overlap of the ground electron state and the ground heavy-hole state are the highest and close to unity, because both of these carriers envelope functions remain symmetrical with respect to the QW axis (Figs. 3 and 4) but represent carriers of different effective masses. As electric field increases,

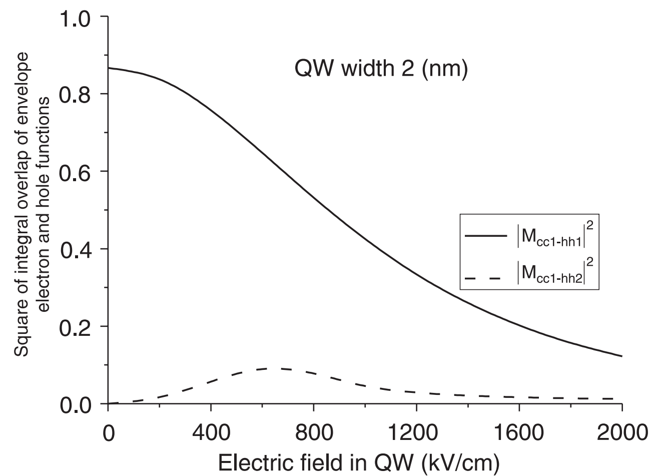

Fig. 9. Dependence of a square of the integral overlap of the envelope electron and the hole functions versus various electric field values for the $Al_{0.15}Ga_{0.85}N$/GaN QW structure with the 2-nm wide well and the 10-nm wide barriers.

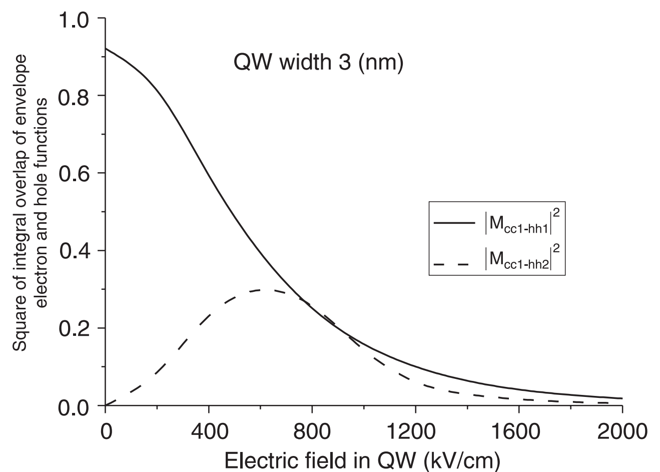

Fig. 10. Dependence of a square of the integral overlap of the envelope electron and the hole functions versus various electric field values for the $Al_{0.15}Ga_{0.85}N$/GaN QW structure with the 3-nm wide well and the 10-nm wide barriers.

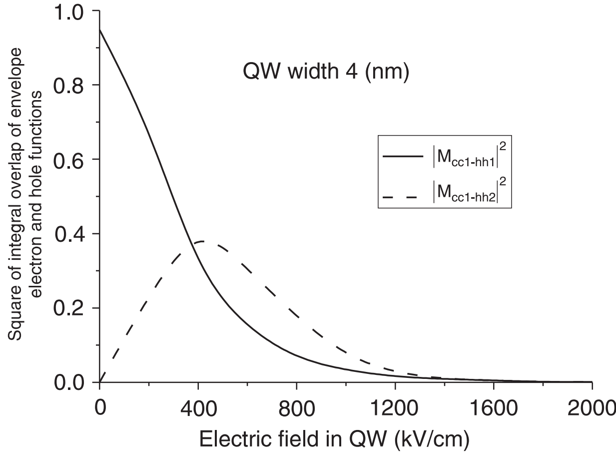

Fig. 11. Dependence of a square of the integral overlap of the envelope electron and the hole functions versus various electric field values for the $Al_{0.15}Ga_{0.85}N$/GaN QW structure with the 4-nm wide well and the 10-nm wide barriers.

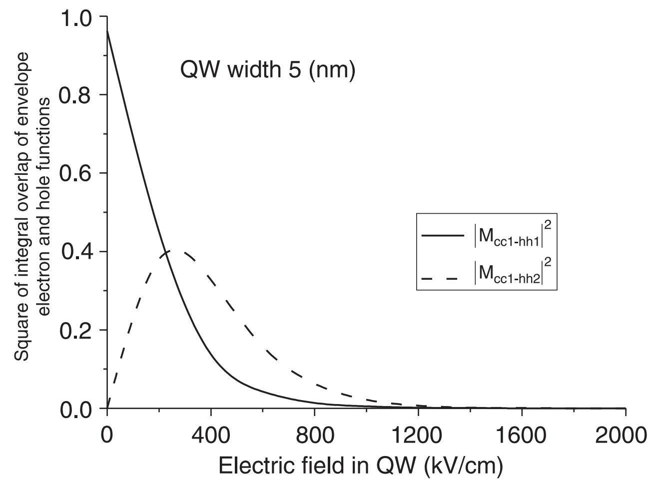

Fig. 12. Dependence of a square of the integral overlap of the envelope electron and the hole functions versus various electric field values for the $Al_{0.15}Ga_{0.85}N$/GaN QW structure with the 5-nm wide well and the 10-nm wide barriers.

there is gradual reduction in square of integral overlap of ground electron state and ground heavy hole state ($|M_{cc1\text{-}hh1}|^2$). However, integral overlap of ground electron state and second heavy hole state ($|M_{cc2\text{-}hh2}|^2$) is increasing to reach a maximum (for lower electric fields in thicker QWs) and then, at electric fields over 700 kV/cm, to gradually reduce to zero as it is the case of $|M_{cc1\text{-}hh1}|^2$. Though $|M_{cc1\text{-}hh2}|^2$ is generally lower than $|M_{cc1\text{-}hh1}|^2$, at large electric fields (dependent on the QW width) and in QW wider than 3 nm its contribution becomes comparable with or even larger than that from $|M_{cc1\text{-}hh1}|^2$. This directly implies that a correct evaluation of optical properties such as recombination rate or absorption coefficient at higher electric fields should also include $|M_{cc1\text{-}hh2}|^2$ which cannot be neglected as it is usually the case.

6. Conclusions

The stress-induced separation of recombining carriers in nitride GaN/(AlGa)N QW devices has been studied in this paper with the aid of the modified **k·p** method. Results show that increasing electric field within QWs causes a shift of the maxima of the electrons and the holes envelope functions in the opposite directions, which is called the quantum confined Stark effect. Theoretical calculations of square integral overlap for $Al_{0.15}Ga_{0.85}N$/GaN QW structure of different QW widths for various electric fields have been carried out to allow further investigation of optical parameters such as recombination rate and absorption coefficient, both dependent on square integral overlap. It has been found out that in wide QWs (5 nm) under a large electric field (0.88 MV/cm) caused in the above QW structures only by stress-induced (piezoelectric) and spontaneous polarization, square of integral overlap of ground electron state and second heavy hole state becomes larger than square integral overlap of ground carrier states. Above phenomena directly implies necessity of including also these second carrier transitions in evaluating correct optical properties of nitride GaN/(AlGa)N QW devices.

Appendix A

Following Chuang and Chang [9,10] the block-diagonalized valence band Hamiltonian for strained wurtzite crystals can be written as follows

$$\hat{H}_{6\times 6} = \begin{bmatrix} F & K_t & -iH_t & 0 & 0 & 0 \\ K_t & G & \Delta - iH_t & 0 & 0 & 0 \\ iH_t & \Delta + iH_t & \lambda & 0 & 0 & 0 \\ 0 & 0 & 0 & F & K_t & iH_t \\ 0 & 0 & 0 & K_t & G & \Delta + iH_t \\ 0 & 0 & 0 & -iH_t & \Delta - iH_t & \lambda \end{bmatrix} = \begin{bmatrix} \hat{H}^U & 0 \\ 0 & \hat{H}^L \end{bmatrix}$$

where

$$F = \Delta_1 + \Delta_2 + \lambda + \theta,$$

$$G = \Delta_1 - \Delta_2 + \lambda + \theta,$$

$$\lambda = \frac{\hbar^2}{2m_0}\left[A_1 k_z^2 + A_2 k_t^2\right] + \lambda_{\in},$$

© 2004 COSiW SEP, Warsaw

$$\lambda_{\in} = -2\varepsilon_{11}\left(D_1 \frac{C_{13}}{C_{33}} - D_2\right),$$

$$\theta = \frac{\hbar^2}{2m_0}\left[A_3 k_z^2 + A_4 k_t^2\right] + \theta_{\in},$$

$$\theta_{\in} = -2\varepsilon_{11}\left(D_3 \frac{C_{13}}{C_{33}} - D_4\right),$$

$$K_t = \frac{\hbar^2}{2m_0} A_5 k_t^2,$$

$$H_t = \frac{\hbar^2}{2m_0} A_6 k_z k_t, \;\; \Delta = \sqrt{2}\Delta_3$$

where A_i are the valence-band effective-mass parameters analogous to the γ_i Luttinger parameters, $\Delta_1 = \Delta_{cr}$ is the crystal-field split energy, $3\Delta_2 = 3\Delta_3 = \Delta_{so}$ is the spin-orbit split-off energy and D_i are the deformation potentials [21]. Values of the above **k·p** parameters for the binary GaN and AlN compounds are listed in Table 2. It should be noted that $H^U = (H^L)^* = (H^L)^T$ and for $k_t = 0$, which is the case in this paper, $H^U = H^L$ (where * is the complex conjugate and ^{T} means transpose of matrix elements).

The bases for the block-diagonalized Hamiltonian are defined as

$$|1\rangle = \alpha^*\left|-\frac{X+iY}{\sqrt{2}}\uparrow\right\rangle + \alpha\left|-\frac{X+iY}{\sqrt{2}}\downarrow\right\rangle,$$

$$|2\rangle = \beta\left|\frac{X-iY}{\sqrt{2}}\uparrow\right\rangle + \beta^*\left|\frac{X+iY}{\sqrt{2}}\downarrow\right\rangle,$$

$$|3\rangle = \beta^*\left|Z\uparrow\right\rangle + \beta\left|Z\downarrow\right\rangle,$$

$$|4\rangle = \alpha^*\left|-\frac{X+iY}{\sqrt{2}}\uparrow\right\rangle - \alpha\left|-\frac{X-iY}{\sqrt{2}}\downarrow\right\rangle,$$

$$|5\rangle = \beta\left|\frac{X-iY}{\sqrt{2}}\uparrow\right\rangle - \beta^*\left|-\frac{X+iY}{\sqrt{2}}\downarrow\right\rangle,$$

$$|6\rangle = -\beta^*\left|Z\uparrow\right\rangle + \beta\left|Z\downarrow\right\rangle,$$

where

$$\alpha = \frac{1}{\sqrt{2}}\exp\left[i\left(\frac{3\pi}{4} + \frac{3\phi}{2}\right)\right]$$

and

$$\beta = \frac{1}{\sqrt{2}}\exp\left[i\left(\frac{\pi}{4} + \frac{\phi}{2}\right)\right].$$

Acknowledgments

This work was supported by the Polish State Committee for Scientific Research (KBN), grants Nos. 7-T11B-073-21 and 4-T11B-014-25.

References

1. F. Bernardini, V. Fiorentini, and D. Vanderbilt, “Spontaneous polarization and piezoelectric constants of III-V nitrides”, *Phys. Rev.* **B56**, R10024-R10027 (1997).
2. A. Zoroddu, F. Bernardini, P. Ruggerone, and V. Fiorentini, “First-principles prediction of structure, energetics, formation enthalpy, elastic constants, polarization, and piezoelectric constants of AlN, GaN, and InN: Comparison of local and gradient-corrected density-functional theory”, *Phys. Rev.* **B64**, 045208–045214 (2001).
3. F. Bernardini and V. Fiorentini, “Polarization-based calculation of the dielectric tensor of polar crystals”, *Phys. Rev. Lett.* **79**, 3958–3961 (1997).
4. F. Bernardini and V. Fiorentini, “Nonlinear macroscopic polarization in III-V nitride alloys”, *Phys. Rev.* **B64**, 085207–085214 (2001).
5. F. Bernardini and V. Fiorentini, “Spontaneous versus piezoelectric polarization in III-V nitrides: Conceptual aspects and practical consequences”, *Phys. Stat. Sol. (b)* **216**, 391–399 (1999).
6. D.A.B. Miller, D.S. Chemla, T.C. Damen, A.C. Gossard, W. Wiegmann, T.H. Wood, and C.A. Burrus, “Band-edge electro-absorption in quantum well structures: The quantum-confined Stark effect”, *Phys. Rev. Lett.* **53**, 2173–2177 (1984).
7. T. Takeuchi, S. Sota, M. Katsuragawa, M. Komori, H. Takeuchi, H. Amano, and I. Akasaki, “Quantum-confined Stark effect due to piezoelectric fields in GaInN strained quantum wells”, *Jpn. J. Appl. Phys.* **36**, L382–385 (1997).
8. A. Thilagam, “Stark shifts of charged particles in semiconductor quantum wells”, *Appl. Phys.* **A64**, 83–89 (1997).
9. S.L. Chuang and C.S. Chang, “**k·p** method for strained wurtzite semiconductors”, *Phys. Rev.* **B54**, 2491–2504 (1996).
10. S.L. Chuang, *Physics of Optoelectronic Devices*, Wiley, New York, 1995.
11. S.L. Chuang and C.S. Chang, “A band-structure model of strained quantum-well wurtzite semiconductors”, *Semicond. Sci. Technol.* **12**, 252–263 (1997).
12. O. Ambacher, J. Majewski, C. Miskys, A. Link, M. Herman, M. Eickhoff, M. Stutzmann, F. Bernardini, V. Fiorentini, V. Tilak, B. Schaff, L.F. Eastman, *J. Phys.: Cond. Matter.* **14**, 3399 (2001).
13. M.E. Levinsthtein, S.L. Rumyantsev, and M.S. Shur, *Properties of Advanced Semiconductor Materials GaN*, *AlN*, *InN*, *BN*, *SiC*, *SiGe*, Wiley, New York, 2001.
14. M. Suzuki, T. Uenoyama, and A. Yanase, “First-principles calculations of effective-mass parameters of AlN and GaN”, *Phys. Rev.* **B52**, 8132–8139 (1995).
15. K. Kim, W.R.L. Lambrecht, and B. Segall, “Elastic constants and related properties of tetrahedrally bonded BN, AlN, GaN, and InN”, *Phys. Rev.* **B53** 16310–16326 (1996).
16. S.H. Park and S.L. Chuang, “Comparison of zinc-blende and wurtzite GaN semiconductors with spontaneous polar-

ization and piezoelectric field effects", *J. Appl. Phys.* **87**, 353–364 (2000).

17. G. Martin, S. Strite, A. Botchkarev, A. Agarwal, A. Rockett, H. Morkoc, W. R.L. Lambrecht, and B. Segall, "Valence-band discontinuity between GaN and AlN measured by X-ray photoemission spectroscopy", *Appl. Phys. Lett.* **65**, 610–612 (1994).
18. J. Han, M.H. Crawford, R.J. Shul, S.J. Hearne, E. Chason, J.J. Figiel, and M. Banas, "Monitoring and controlling of strain during MOCVD of AlGaN for UV optoelectronics", *MRS Internet J. Nitride Semicond. Res.* **4S1**, Paper G7.7 (1999).
19. L.T. Romano, C.G. Van de Walle, W. Ager III, W. Götz, and R.S. Kern, "Effect of Si doping on strain, cracking, and microstructure in GaN thin films grown by metalorganic chemical vapour deposition", *J. Appl. Phys.* **87**, 7745–7752 (2000).
20. H.M. Wang, J.P. Zhang, C.Q. Chen, Q. Fareed, J.W. Yang, and A. Khan, "AlN/AlGaN superlattices as dislocation filter for low-threading-dislocation thick AlGaN layers on sapphire", *Appl. Phys. Lett.* **81**, 604–606 (2002).
21. G.L. Bir and G.E. Pikus, *Symmetry and Strained-Induced Effects in Semiconductors*, Wiley, New York, 1974.

 © 2004 COSiW SEP, Warsaw